

## Dynamical properties of one-dimensional antiferromagnets: A Monte Carlo study

J. Deisz

*Department of Physics, The Ohio State University, Columbus, Ohio 43210  
and Department of Physics, Montana State University, Bozeman, Montana 59717\**

M. Jarrell

*Department of Physics, University of Cincinnati, Cincinnati, Ohio 45221*

D. L. Cox

*Department of Physics, The Ohio State University, Columbus, Ohio 43210*

(Received 24 June 1992; revised manuscript received 18 March 1993)

A combination of world-line quantum Monte Carlo and maximum-entropy methods is used to calculate the dynamic structure factor  $S_{\alpha\alpha}(q, \omega)$  for one-dimensional antiferromagnets. A comparison to exact results demonstrates that qualitative features of spectra are reproduced, but are broadened. The broadening is frequency dependent with low-frequency features being reproduced most accurately. Peak positions are well described. Results for the Heisenberg model with  $S \leq 2$  demonstrate the qualitative difference between the dynamics of half-integer and integer spins predicted by Haldane. From the positions of the low-temperature  $q = \pi$  peaks quantitative estimates are produced for the  $S = 1$  and 2 gaps. The  $q = \pi$  peak position for  $S = 1$  increases with temperature in agreement with experiment. When on-site anisotropy is included for  $S = 1$  a gap splitting results that resembles that found for NENP  $[\text{Ni}(\text{C}_2\text{H}_8\text{N}_2)_2\text{NO}_2\text{ClO}_4]$ .

### I. INTRODUCTION

There are several compounds that behave as one-dimensional antiferromagnets, at least to very low temperatures. Examples include  $\text{CuCl}_2 \cdot 2\text{N}(\text{C}_5\text{H}_5)$  (Ref. 1) and  $\text{KCuF}_3$  (Ref. 2) with spin  $S = \frac{1}{2}$  and  $\text{CsNiCl}_3$ , NENP  $[\text{Ni}(\text{C}_2\text{H}_8\text{N}_2)_2\text{NO}_2\text{ClO}_4]$ ,<sup>4</sup> and  $\text{VaAgCl}_2$  (Ref. 5) with  $S = 1$ . Much of the motivation for recent experimental and theoretical studies of one-dimensional antiferromagnets is due to Haldane who made the surprising conjecture that one-dimensional integer spin Heisenberg antiferromagnets have excitation gaps while half-integer spins are gapless in the thermodynamic limit.<sup>6</sup> This conjecture has been verified by both experimental<sup>3-5</sup> and numerical studies.<sup>7-9</sup>

Numerical studies are often limited to determining the lowest eigenvalue for a given set of quantum numbers (i.e., spin and momentum).<sup>7,8</sup> This is adequate for determining whether or not an excitation gap exists and, if so, the gap's magnitude. However, the line shape observed in inelastic neutron-scattering experiments is directly related to  $S(q, \omega)$ , the dynamic structure factor, which often has spectral intensity for more than one excitation. This is especially true in one dimension. For example, the  $S = \frac{1}{2}$  antiferromagnetic Heisenberg model has a broad continuum of excited states accessible from the ground state for each value of  $q$ .<sup>10</sup> Full diagonalization and the Lanczos method can be used to exactly calculate  $S(q, \omega)$  for zero temperature, but these methods are restricted to small system sizes, on the order of 36 sites for  $S = \frac{1}{2}$  (Ref. 11) and smaller for larger values of  $S$ . The temperature dependence of  $S(q, \omega)$  presents a further complication, but, as we will see, is of experimental

relevance.

Previously we reported results for the dynamical structure factor,  $S(q, \omega)$ , for the one-dimensional  $S = \frac{1}{2}$  and 1 antiferromagnetic Heisenberg models obtained with a combination of the world-line quantum Monte Carlo and maximum entropy methods.<sup>12</sup> Our results show the qualitative difference between the  $S = \frac{1}{2}$  and 1 excitation spectra predicted by Haldane. The triplet excitation gap for  $S = 1$  was calculated to be  $0.4J$ , in good quantitative agreement with the results obtained using other methods.<sup>7-9</sup> For  $S = \frac{1}{2}$  our results provide a good description of the inelastic neutron-scattering line shape for  $\text{CuCl}_2 \cdot 2\text{N}(\text{C}_5\text{H}_5)$ . These results are encouraging as the technique is applicable to large system sizes (we use up to 128 sites here, up to  $64 \times 64$  sites have been used for dynamical studies of the two-dimensional  $S = \frac{1}{2}$  Heisenberg antiferromagnet<sup>13</sup>). Further, the temperature dependence of  $S(q, \omega)$  can be determined. The primary limitation to this method is the finite resolution with respect to frequency that can be achieved, i.e.,  $S(q, \omega)$  results are broadened with respect to the exact functional form. The broadening is large for high frequencies, but is small for low frequencies allowing for accurate nonperturbative results in that regime.

In this paper we report improved results for  $S = \frac{1}{2}$  and 1 and new results for  $S = \frac{3}{2}$  and 2 and for  $S = 1$  with on-site anisotropy. The most important results are the following. Using system sizes of up to 128 sites we estimate the  $S = 2$  gap to be  $0.08J$  in the thermodynamic limit.  $S = \frac{3}{2}$  and 2 results are shown to approach the classical limit where  $S(q, \omega)$  is dominated by a single mode which is gapless at  $q = \pi$ . For  $S = 1$  the  $q = \pi$  peak position increases with temperature in agreement with experimental

results. When on-site anisotropy is included for  $S=1$ , a gap splitting for  $q=\pi$  results which describes the same found for NENP. As  $q$  decreases the peak splitting also decreases which is also observed experimentally.

Before presenting these results, we provide a brief description of the method (a more detailed description appears elsewhere<sup>14</sup>). We compare our results to exact results for the Ising and  $xy$  models in order to gauge the method's accuracy. This comparison shows that low-frequency features are reproduced accurately, but high-frequency features are substantially broadened. Regardless, peak positions are given accurately.

## II. METHOD FOR OBTAINING $S(q, \omega)$

World-line quantum Monte Carlo simulations<sup>15</sup> are used to stochastically evaluate the imaginary-time correlation function

$$S_{zz}(q, \tau) = \frac{1}{2} \langle e^{H\tau} S_z(q) e^{-H\tau} S_z(-q) \rangle \\ \simeq \frac{1}{2} \sum_r e^{-iqR} \overline{S_z(R, \tau) S_z(R=0, \tau=0)} \quad (1)$$

at a finite set ( $\sim 50$ ) of evenly spaced  $\tau$  values between 0 and  $\beta/2$  where  $\beta=1/(k_B T)$ . (The subscript  $zz$  indicates the direction in spin space for correlations. We omit the subscript in this general discussion.) The average indicated by the overbar on the right-hand side of Eq. (1) is taken over  $\sim 10^4$  configurations of the  $\sim 10^8$  configurations generated by the world-line Monte Carlo simulation. As we shall discuss in more detail, the approximation becomes exact in the limit of infinite Monte Carlo sweeps and zero time slice spacing  $\Delta\tau$ .

The statistical errors due to finite Monte Carlo sampling are described by the covariance matrix

$$C(\tau, \tau') = \overline{[S(q, \tau) - \overline{S(q, \tau)}][S(q, \tau') - \overline{S(q, \tau')}]}. \quad (2)$$

There are strong correlations between fluctuations at different imaginary times  $\tau$  and  $\tau'$ , thus nondiagonal elements ( $\tau \neq \tau'$ ) of the covariance matrix are retained. The eigenvalues of  $C(\tau, \tau')$ ,  $\lambda_i$ , describe the error bars  $\sigma_i$  of statistically independent quantities  $S_i(q)$ , which are linear combinations of  $S(q, \tau)$  at different values of  $\tau$ . Explicitly

$$\sigma_i = \sqrt{\lambda_i / (N-1)} \quad (3)$$

where  $N$  is the number of samples.

There are also systematic, nonstatistical, errors associated with the world-line Monte Carlo evaluation of Eq. (1). These errors are of order  $(\Delta\tau)^2$ , where  $\Delta\tau$  is the step size between  $\tau$  values in the Trotter decomposition of the thermodynamic density matrix.<sup>15</sup> Typically we take  $\Delta\tau=0.25J^{-1}$  where  $J$  is the exchange constant. For the  $xy$  and  $S=\frac{1}{2}$  antiferromagnetic Heisenberg models we did not find significant changes in our dynamical results when using smaller values of  $\Delta\tau$ .

The imaginary-time correlation function is related to the dynamic structure factor by

$$S(q, \tau) = \frac{1}{2\pi} \int_0^\infty e^{-\omega\tau} (1 + e^{-\beta\omega}) S(q, \omega) d\omega \quad (4)$$

or

$$S_i(q) = \int_0^\infty (i|\tau)_\omega S(q, \omega) d\omega, \quad (5) \\ S_i(q) = [i|S(q, \tau)]$$

where  $(i|\tau)_\omega$  is the  $\omega$ -dependent scalar product of the  $i$ th eigenvector of the covariance matrix and the set of kernels

$$e^{-\omega\tau} (1 + e^{-\beta\omega}) / (2\pi)$$

for the discrete set of  $\tau$  values at which  $S(q, \tau)$  is evaluated. However, the extraction of  $S(q, \omega)$  from Eq. (5) is ill posed for two reasons: (1) an infinite set of functions  $S(q, \omega)$  satisfies Eq. (5) for the discrete and finite set of  $S_i(q)$  results and (2) the Monte Carlo  $S_i(q)$  values are correct only to within their error bars  $\sigma_i$ . In addition, the transformation matrix between  $S(q, \tau)$  and  $S(q, \omega)$  becomes exponentially singular as the number of  $\omega$  and  $\tau$  points increases in a discretized approximation to Eq. (5). Thus the direct inversion of Eq. (5) using a finite  $\omega$  grid is uncontrolled.

In order to overcome these difficulties, we employ the maximum entropy method which provides an approximate result<sup>16-18</sup> with the biasing necessary to produce a unique result being towards a predefined "default model"  $m(q, \omega)$ . Briefly, the maximum entropy method works as follows. The entropy functional is defined as

$$I[\tilde{S}(q, \omega)] = - \int_0^\infty \tilde{S}(q, \omega) \ln \left[ \frac{\tilde{S}(q, \omega)}{m(q, \omega)} \right] - \tilde{S}(q, \omega) d\omega, \quad (6)$$

which is the information theory quantity describing the difference between the trial function  $\tilde{S}(q, \omega)$  and  $m(q, \omega)$ . The information contained in the Monte Carlo data is introduced through the  $\chi^2$  term given by

$$\chi^2[\tilde{S}(q, \omega)] = \sum_i \frac{[S_i(q) - \int_0^\infty (i|\tau)_\omega \tilde{S}(q, \omega) d\omega]^2}{\sigma_i^2}, \quad (7)$$

which describes how close  $\tilde{S}(q, \omega)$  comes to reproducing the Monte Carlo results  $S_i(q)$  to within the error bars  $\sigma_i$ . Finally, the trial function  $\tilde{S}(q, \omega)$  which maximizes the functional

$$\alpha I - \chi^2 \quad (8)$$

is chosen as the approximate result for  $S(q, \omega)$ .

In Eq. (8) the Lagrange multiplier  $\alpha$  determines the relative weight given to the entropy ( $I$ ) and  $\chi^2$  terms. A small value of  $\alpha$  favors a small  $\chi^2$ , and thus the result for  $S(q, \omega)$  provides a close fit to the Monte Carlo results for  $S_i(q)$ . A large value of  $\alpha$  favors a large entropy, which will then drive the output  $S(q, \omega)$  to the "default model"  $m(q, \omega)$  (the maximum of  $I[\tilde{S}(q, \omega)]$  occurs for  $\tilde{S}(q, \omega) = m(q, \omega)$ ).

There is no rigorous prescription for determining a "correct" value for  $\alpha$  in the sense that no value for  $\alpha$  will lead to the exact result. It is desirable that the choice for  $\alpha$  allows for a good fit to the data, but without overfitting such that spurious statistical error induced features show

up in  $S(q, \omega)$ . In this work  $\alpha$  is chosen by maximizing a probability distribution as is described by Gubernatis *et al.*<sup>18</sup> When  $\alpha$  is chosen this way it typically ranges between 0.1 and 10. The smaller values of  $\alpha$  are chosen when spectral intensity is concentrated at low frequency. This leads to a  $\chi^2$  value between  $N_\tau/2$  and  $N_\tau$  where  $N_\tau$  is the number of imaginary-time data points. Thus, loosely speaking, the maximum entropy method is equivalent to fitting the Monte Carlo data to within an error bar on average while staying as close as possible to the default model  $m(q, \omega)$ .

### III. COMPARISON TO EXACT RESULTS

#### A. The Ising model

The  $S = \frac{1}{2}$  Ising Hamiltonian is given by

$$H = J \sum_i S_i^z S_{i+1}^z \quad (9)$$

for which the correlation functions can be determined exactly at any temperature. The transverse correlation function is given by

$$S_{xx}(R, \tau) = S_{yy}(R, \tau) = \frac{1}{2} \langle e^{\tau H} S^x(R) e^{-\tau H} S^x(R=0) \rangle \quad (10)$$

$$= \frac{1}{4} \langle e^{\tau H} S^+(R) e^{-\tau H} S^-(R=0) \rangle, \quad (11)$$

where  $S^+$  and  $S^-$  are spin raising and lowering operators. This correlation function probes states with single spin flips relative to equilibrium. These flips change the energy by  $J$ , 0, or  $-J$ , so  $S_{xx}(q, \omega)$  is nonzero for these three values of frequency. For a periodic chain with  $N$  sites the exact result for  $S_{xx}(q, \omega)$  is

$$S_{xx}(q, \omega) = \frac{\pi}{16 \cosh^2(\beta J/4)} \frac{1 + e^{-(N-2)/\xi}}{1 + e^{-N/\xi}} \times \{ e^{\beta J/2} \delta(\omega - J) + e^{-\beta J/2} \delta(\omega + J) + 2 \tanh[(N/2 - 1)/\xi] \delta(\omega) \}, \quad (12)$$

where

$$\xi = \{ \ln[\coth(\beta J/4)] \}^{-1}. \quad (13)$$

This result is  $q$  independent, so the variable  $q$  is omitted in this discussion.

Since the dynamical method used here is inexact, the final result for  $S_{xx}(\omega)$  will depend on (1) the default model  $m(\omega)$  used in the entropy functional of Eq. (6), (2)  $N_\tau$ , the number of  $\tau$  values at which  $S_{xx}(\tau)$  is evaluated, and (3) the statistical accuracy of these  $S_{xx}(\tau)$  values, which is determined by the number of samples. In order to examine the sensitivity of our results to (1)–(3), we first choose a reference simulation with temperature  $T = J/6$  ( $\xi \sim 10$ ),  $N = 64$  sites and  $m = 48$  time slices producing  $N_\tau = m/2 + 1 = 25$  independent  $\tau$  values at which to evaluate  $S_{xx}(\tau)$ .  $10^4$  samples are taken with 100 complete Monte Carlo lattice sweeps of configuration updates between each sample.

Figure 1(a) shows two choices for the default model,  $m(\omega)$ . Like  $S_{xx}(\omega)$ ,  $m(\omega)$  is uniquely defined only for  $\omega > 0$ ;  $m(-\omega)$  is taken to be  $e^{-\beta\omega} m(\omega)$ . The dashed line

is a constant from  $\omega=0$  to an arbitrarily chosen cutoff at  $\omega_c = 2J$ . The normalization is set by requiring

$$\frac{1}{2\pi} \int_0^\infty (1 + e^{-\beta\omega}) m(q, \omega) d\omega = S_{xx}(\tau=0) = \langle (S_x)^2 \rangle / 2 = \frac{1}{8}. \quad (14)$$

The solid line is the three-sum-rule default. It satisfies Eq. (14) and two additional constraints:

$$\frac{1}{2\pi} \int_0^\infty \omega^{-1} (1 - e^{-\beta\omega}) m(\omega) d\omega = \chi_{xx}, \quad (15)$$

where  $\chi_{xx}$  is the transverse magnetic susceptibility, and

$$\frac{1}{\pi} \int_0^\infty \omega (1 - e^{-\beta\omega}) m(\omega) d\omega = -\langle S_0^z S_1^z \rangle. \quad (16)$$

Equations (14)–(16) do not uniquely specify  $m(\omega)$ . In the spirit of the rest of this work we require that

$$\int_0^\infty [-m(\omega) \ln m(\omega) + m(\omega)] d\omega \quad (17)$$

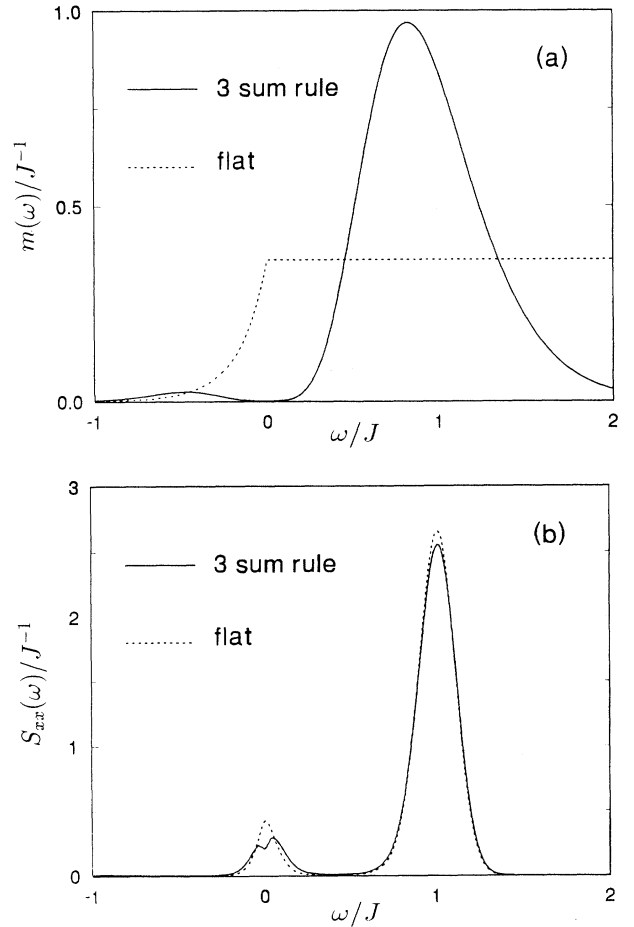


FIG. 1. (a) Two default models  $m(\omega)$  applied to the Ising model. (b) The subsequent results for  $S_{xx}(\omega)$ . Although the default models are quite different, the final results for  $S_{xx}(\omega)$  are nearly the same. Thus the arbitrariness in the choice of default model does not pose a practical difficulty for this method.

TABLE I. Comparison of exact peak intensities to peak intensities obtained with Monte Carlo and maximum entropy for the Ising model.

		Intensities	
		$\omega=0$	$\omega=J$
Exact	$T=J/6$	0.0707	0.7129
Figure 1(b)	Flat default	$0.065\pm 0.016$	$0.717\pm 0.017$
	Three-sum-rule default	$0.066\pm 0.017$	$0.716\pm 0.018$
Figure 2(a)		$0.0725\pm 0.0005$	$0.7111\pm 0.0004$
Figure 2(b)		$0.0714\pm 0.0006$	$0.7123\pm 0.0006$
Exact	$T=J/4$	0.1649	0.6092
Figure 3		$0.160\pm 0.022$	$0.612\pm 0.021$

is maximized subject to the constraints of Eqs. (14)–(16).

The results for  $S_{xx}(\omega)$  are shown in Fig. 1(b). The two default models produce results that are very similar. However, there is a “glitch” at  $\omega=0$  for the result produced with the three-sum-rule default model. This glitch is due to the suppression of  $\omega=0$  intensity in the three-sum-rule default model. We note that the three sum rules of Eqs. (14)–(16) do not contain enough information to describe more than a single peak, but the  $S_{xx}(\tau)$  data contain the additional information necessary to resolve the two-peak structure.

The peak positions in Fig. 1(b) correspond to the positions of the delta functions in the exact result. Table I shows that each peak’s integrated intensity is in good agreement with the exact weights of the delta functions with the error bars on the integrated intensities calculated following Gubernatis *et al.*<sup>18</sup>

The broadening is substantial, on the order of  $0.3J$ . It is worth considering whether or not we can estimate the maximum entropy resolution as this will have bearing on the interpretation of results where the spectrum is unknown and nontrivial. To that end we have tried the following: (1) replace the  $S_i(q)$  data with that which would be produced by a single mode at energy  $\omega_0$  with noise added according to the covariance matrix and (2) the width of the subsequent maximum entropy result, using the same value for  $\alpha$  as for the actual spectrum, is the resolution at  $\omega_0$ .

This procedure suggests that the broadening of a feature at  $\omega=J$  is about  $0.1J$  and  $0.02J$  for  $\omega=0$ . Thus, this method underestimates the broadening that is actually observed. Apparently this procedure does not take into account the increased difficulty of resolving a multip peaked structure. In Sec. III B, however, we show that this procedure for estimating the broadening works for a simpler single-peak structure.

Figure 2(a) shows the improvement made in the results when the statistical uncertainty of  $S_{xx}(\tau)$  values is reduced by a factor of 2, which is accomplished by increasing the number of samples from  $10^4$  to  $4\times 10^4$ . The broadening of the delta functions decreases substantially.

Data in Table I show that the statistical uncertainties of the integrated peak intensities from Fig. 2(a) are few error bars away from the exact values. Such discrepancies can be expected. Systematic errors in the Monte Carlo simulation are of the order  $e^{-N/\xi} = e^{-6.4} \sim 0.2\%$

due to the omission of “winding numbers” different from zero.<sup>19</sup> Nonzero winding numbers describe the traversal of spin flips around the periodic lattice between  $\tau=0$  and  $\beta$ . Properly including nonzero winding numbers in a world-line Monte Carlo simulation is difficult except for very small lattices.

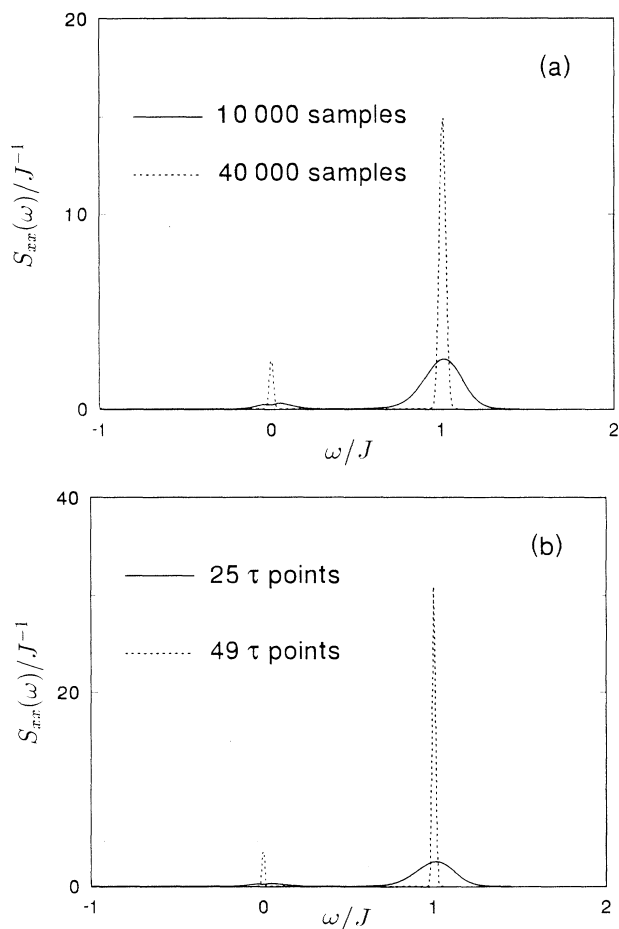


FIG. 2. (a) For the Ising model increasing the number of samples from  $10^4$  to  $4\times 10^4$  improves the statistical accuracy of  $S_{xx}(\tau)$  results. A result for  $S_{xx}(\omega)$  is then produced which is closer to the exact delta function peaks. (b) Increasing the number of  $\tau$  values from 25 to 49 also leads to an improved result.

Figure 2(b) shows the improvement made when 49  $\tau$  points are used instead of 25. The broadening is substantially reduced upon increasing the number of  $\tau$  points. The uncertainty in the integrated peak intensities is also substantially decreased as shown in Table I.

These results show that reducing the statistical uncertainty and increasing the number of  $\tau$  points is more important for producing good results for  $S_{xx}(\omega)$  than the choice for the default model,  $m(\omega)$ . This is helpful because increasing the precision and the number of  $\tau$  points are well-controlled aspects of this method, while the choice for  $m(\omega)$  is essentially arbitrary. The convergence towards the exact result seems remarkably fast as the controllable parameters are improved. However, a similar analysis for the other models in this study showed a much slower rate of convergence with increasing sample size and decreasing  $\Delta\tau$ . We suspect that the rapid convergence for the Ising model is due to the relative simplicity of its spectrum.

Results for  $T=J/4$  ( $\xi \sim 3$ ) are compared to those for  $T=J/6$  in Fig. 3. Each result is formed with the same number of  $\tau$  points (25) and samples ( $10^4$ ). The peak intensities change (see Table I) in correspondence to the change in the exact result with the increased spin disorder for  $T=J/4$  leading to more  $\omega=0$  intensity. The maximum entropy broadening for  $T=J/4$  appears to be similar, but not identical to that for  $T=J/6$ . The temperature dependence of maximum entropy broadening is even more problematic for the  $xy$  model.

### B. The $xy$ model

The  $xy$  Hamiltonian is given by

$$H = J \sum_i (S_i^x S_{i+1}^x + S_i^y S_{i+1}^y) \\ = \frac{J}{2} \sum_i (S_i^+ S_{i+1}^- + S_i^- S_{i+1}^+). \quad (18)$$

Via the Jordan-Wigner transformation, this Hamiltonian can be written as<sup>20</sup>

$$H = \frac{J}{2} \sum_i (c_i^\dagger c_{i+1} + c_{i+1}^\dagger c_i) \\ + \frac{J}{2} \left[ \exp \left[ i\pi \sum_{j=1}^{N-1} c_j^\dagger c_j \right] - 1 \right] (c_N^\dagger c_1 + c_1^\dagger c_N), \quad (19)$$

where the creation and annihilation operators are Fermion operators. The last term in Eq. (19), which is absent for open boundary conditions, is of order  $1/N$  compared to the first term. Ignoring the endpoint term, upon Fourier transforming we obtain the momentum space form

$$H = \sum_q \epsilon_q c_q^\dagger c_q, \quad \epsilon_q = J \cos q. \quad (20)$$

In contrast to the Ising model, the excitation spectrum of the  $xy$  Hamiltonian is continuous in the thermodynamic limit. The dynamic structure factor makes clear this distinction. For the  $xy$  model  $S_{zz}(q, \omega)$  is given by

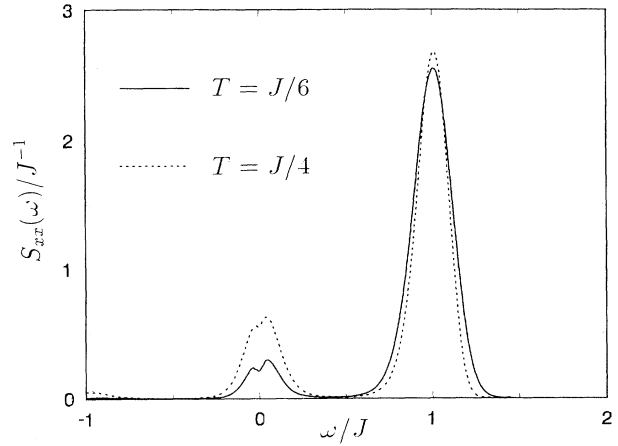


FIG. 3. Temperature dependence of  $S_{xx}(\omega)$  for the Ising model. Upon increasing the temperature from  $J/6$  to  $J/4$  the peak amplitudes change in accordance with the exact result. The maximum entropy broadening of the  $\delta$  functions at  $\omega=0$  and  $J$  does show some variation between these two temperatures.

$$S_{zz}(q, \omega) = \frac{\pi}{N} \sum_{q'} f(\epsilon_{q'}) [1 - f(\epsilon_{q+q'})] \\ \times \delta[\omega - (\epsilon_{q+q'} - \epsilon_{q'})], \quad (21)$$

where  $f(\epsilon_q)$  is the fermi distribution function,

$$f(\epsilon_q) = (e^{\beta\epsilon_q} + 1)^{-1}. \quad (22)$$

Figure 4(a) shows  $S_{zz}(q=\pi, \omega)$  for 64 sites. The delta function peaks have been broadened by convolution with a Gaussian of width  $0.02J$  [recall that peak positions are accurate to only  $\sim J/64$  because the last term is ignored in Eq. (19)].

This dynamical method cannot reproduce the discrete spectrum of the finite-size system shown in Fig. 4(a); the information content of that spectrum is large with respect to any slowly varying default model,  $m(\omega)$ . Instead the maximum entropy method produces a convolution of the exact  $S_{zz}(q, \omega)$  with an *a priori* unknown resolution function. In order to characterize the broadening, we shall compare to results obtained with a Gaussian resolution function. Figure 4(b) shows a convolution of the exact spectrum of Fig. 4(a) with a Gaussian resolution function of width  $\Delta\omega = 0.5J$ , i.e.,

$$S_{\text{convoluted}}(q, \omega) = \frac{2}{\sqrt{\pi}\Delta\omega} \int_0^\infty d\omega' e^{-[(\omega'-\omega)/(\Delta\omega/2)]^2} \\ \times S_{\text{exact}}(q, \omega'). \quad (23)$$

Shown with the broadened spectrum is the exact  $T=0$ ,  $N \rightarrow \infty$  result<sup>21</sup>

$$S_{zz}(q, \omega) = \frac{2\Theta[\omega - J \sin(q)]\Theta[2J \sin(q/2) - \omega]}{\sqrt{4J^2 \sin^2(q/2) - \omega^2}}, \quad (24)$$

where  $\Theta(x) = 0$  for  $x < 0$  and  $\Theta(x) = 1$  for  $x > 0$ . One difference between exact  $N \rightarrow \infty$  are broadened  $N = 64$  re-

sults is the smearing of the van Hove singularity at  $\omega=2J$  into a hump by the convolution process. The smearing of singular features turns out to be a limitation of the maximum entropy method.

In Fig. 5 the maximum entropy result and the convolution of the exact result for  $S_{zz}(q, \omega)$  are compared. The Monte Carlo simulations were performed for 64 site lattices with  $T=J/18$ . The Trotter step  $\Delta\tau$  is  $\frac{3}{16}J^{-1}$  yielding 49 independent  $\tau$  points for  $S_{zz}(q, \tau)$ .  $2 \times 10^4$  samples were taken. We chose the convolution width by requiring the maximum intensities of the convolution and the Monte Carlo results to be equal. There is poor agreement between the Gaussian broadened exact result and the maximum entropy result for  $q=\pi$  [Fig. 5(a)]. However, this provides a rough estimate for the accuracy of the Monte Carlo result ( $\Delta\omega \approx 0.5J$ ). There is better agreement for the spectrum at  $q=\pi/4$  [Fig. 5(b)] where  $\Delta\omega$  is the fairly small value  $0.07J$ . The difference between  $q=\pi$ ,  $\pi/4$  is that for  $q=\pi/4$  the bulk of the spectral weight lies at lower frequencies than the spectral weight for  $q=\pi$ . This demonstrates an important aspect of this

dynamical method: better accuracy is achieved for lower frequency features.

This can be justified as follows. High-frequency spectral weight is suppressed in imaginary time  $\tau$  [see Eq. (4)]. Except for small  $\tau$  values ( $\tau < \omega^{-1}$ ), high-frequency spectral weight is swamped by statistical noise in the Monte Carlo results for  $S(q, \tau)$ . In contrast, low-frequency contributions are statistically significant for many  $\tau$  values.

We have repeated the calculation of Sec. III A, where we unsuccessfully attempted to extract the maximum entropy broadening by observing the line shape when single-mode data is substituted for  $S_i(q)$ . For  $q=\pi$  this suggests a frequency-dependent broadening which is  $0.3J$  for  $\omega=2J$ . Like the Ising model this underestimates the broadening actually observed. However, for the narrow spectrum at  $q=\pi/4$ , the single mode data is broadened by  $0.08J$  which corresponds to the broadening which is used to make the exact result resemble the maximum en-

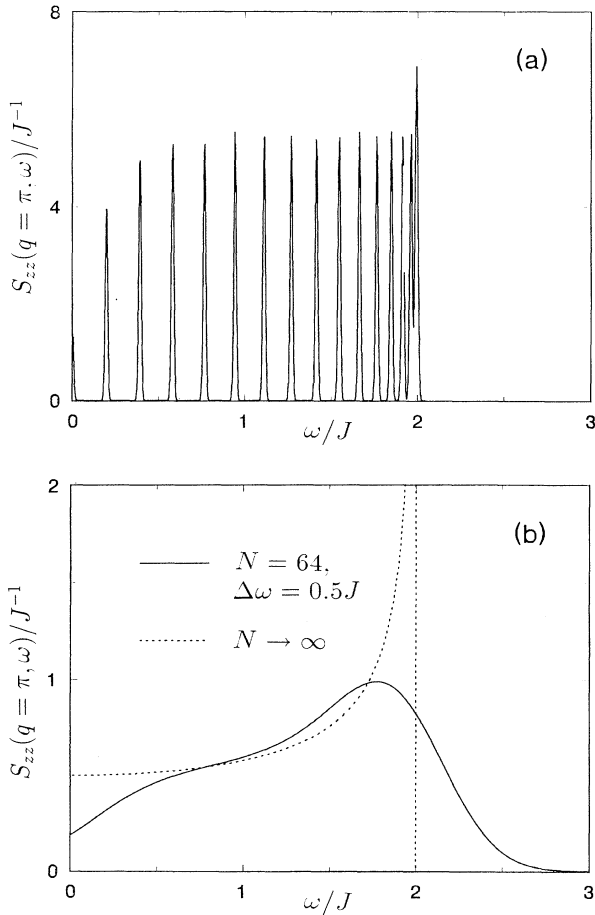


FIG. 4. (a) The exact discrete spectrum for the  $xy$  model with 64 sites. (b) The exact result in the thermodynamic limit versus the Gaussian convolution of the 64-site result with a broadening width  $\Delta\omega=0.5J$ .

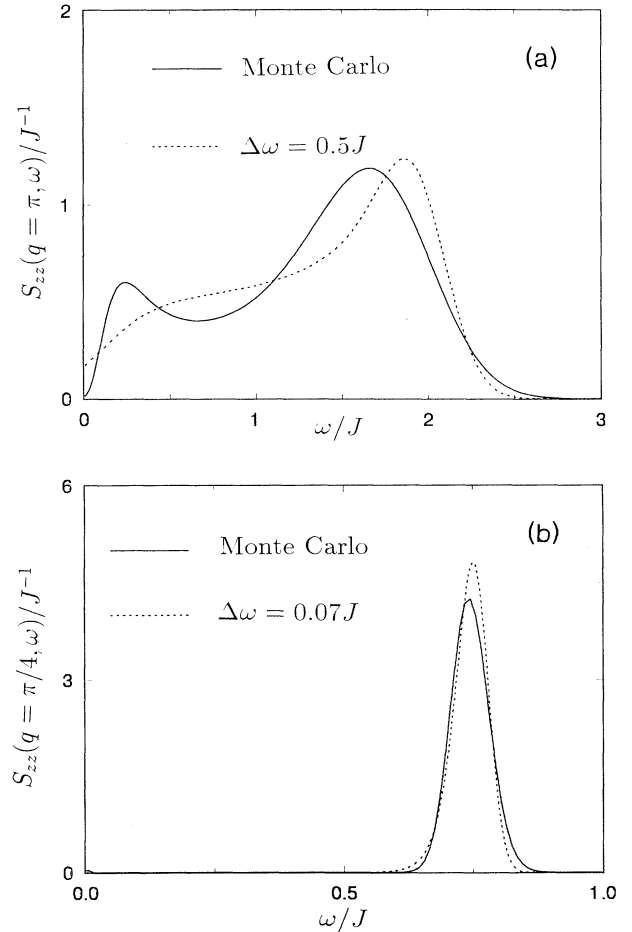


FIG. 5. (a) Monte Carlo result versus convolution of exact 64-site result ( $\Delta\omega=0.5J$ ) for  $S_{zz}(q=\pi, \omega)$ . The qualitative features of the broadened spectrum are reproduced by the Monte Carlo result. (b)  $S_{zz}(q=\pi/4, \omega)$ . A convolution width of only  $0.07J$  is used and agrees very well with the Monte Carlo result. This demonstrates the accuracy of this method at low frequencies.

ropy result. Thus, when the result is a single peak we are able to estimate the amount of broadening. This will be useful later when we show that the widths of certain spectra require a multimode description as maximum entropy broadening of a single mode alone does not explain the observed width.

The convergence tests used for the Ising model (Fig. 2) have been duplicated for the  $xy$  model, but we do not display all of the results here. We find that improving the statistical accuracy or increasing the number of  $\tau$  points decreases the maximum entropy broadening for the  $xy$  model results. However, the improvement in the results is not as exceptional as was found for the Ising model. When  $N_\tau$  or the number of samples is doubled, the reduction in broadening is less than 20%, while the corresponding decrease in the Ising model calculations is as much as 90%.

The temperature dependence of the  $xy$  model results are more problematic than for the Ising model. Figure 6 shows a comparison of  $T=J/12$  and  $J/18$  results. The exact results [obtained from Eq. (21)] change little for this change in temperature, but the Monte Carlo results change substantially. Since the broadening changes are due to this method, the physical temperature broadening cannot be deduced. This is discouraging because the possibility of describing the temperature dependence of line shapes is of experimental relevance and is one of the main advantages, in principle, of this method. Hopefully, more powerful computers or more efficient algorithms or both will provide the increase in precision needed for treating the temperature dependence of broadening. The temperature dependence of the Kondo peak in the spectral function for the impurity Anderson model is well described with the determinantal Monte Carlo and maximum entropy methods,<sup>18</sup> thus some optimism is justified.

The in-plane correlation function  $S_{xx}(q, \omega) = S_{yy}(q, \omega)$

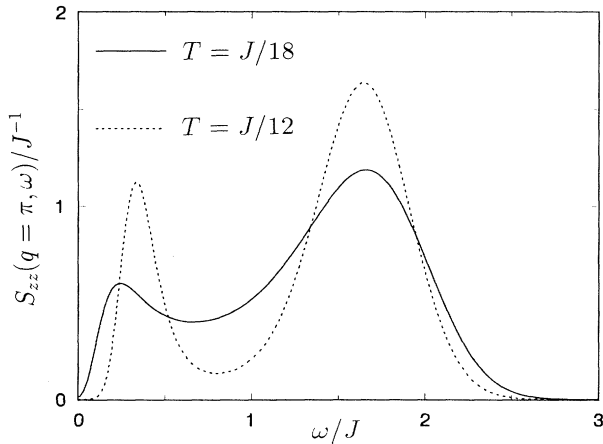


FIG. 6. Temperature dependence of maximum entropy broadening for the  $xy$  model.  $S_{zz}(q = \pi, \omega)$  changes substantially between  $T=J/12$  and  $J/18$ . However, the corresponding exact results (not shown) change very little. This suggests that the method is limited with respect to quantitative studies of the temperature dependence of broadening.

is also of interest for the  $xy$  model. Unlike  $S_{zz}(q, \omega)$ ,  $S_{xx}(q, \omega)$  has not been determined exactly. Relevant work includes that of McCoy, Barouch, and Abraham,<sup>22</sup> Luther and Peschel,<sup>23</sup> and Müller *et al.*<sup>24</sup>

Shown in Fig. 7 is  $S_{xx}(q = \pi, \omega)$  which has a strong temperature dependence. Here a strong temperature dependence is expected because spectral weight is concentrated at frequencies lower than the temperature. This temperature dependence makes it difficult to obtain the asymptotic ( $\omega \rightarrow 0$ ) behavior of  $S_{xx}(q = \pi, \omega)$  for  $T=0$ . The suggested form  $S_{xx}(q = \pi, \omega) \propto \omega^{-1.5}$  (Ref. 24) is displayed in Fig. 7. Our results are less singular than  $\omega^{-1.5}$ , but this can be attributed to finite-temperature broadening or maximum entropy broadening or both.

#### IV. THE HEISENBERG MODEL

The isotropic antiferromagnetic Heisenberg model Hamiltonian is given by

$$H = J \sum_i \mathbf{S}_i \cdot \mathbf{S}_{i+1}, \quad J > 0. \quad (25)$$

An exact solution for  $S_{zz}(q, \omega)$  has not been found for the Heisenberg model for any value of the spin. Here we give results for spin values  $S = \frac{1}{2}$ , 1,  $\frac{3}{2}$ , and 2. Results are for 64-site systems with  $m = 96$  time slices and  $T = J/24$ , except where indicated otherwise.

##### A. $S = \frac{1}{2}$

The Schrödinger equation for the one-dimensional Heisenberg model has been solved in the thermodynamic limit only for  $S = \frac{1}{2}$ .<sup>25</sup> However, an analytic solution for  $S_{zz}(q, \omega)$  has not been produced because the wave functions are too complicated. des Cloizeaux and Pearson<sup>26</sup> have shown that for each  $q$  value there is a continuum of excited states which contribute to  $S_{zz}(q, \omega)$  for  $T=0$ .

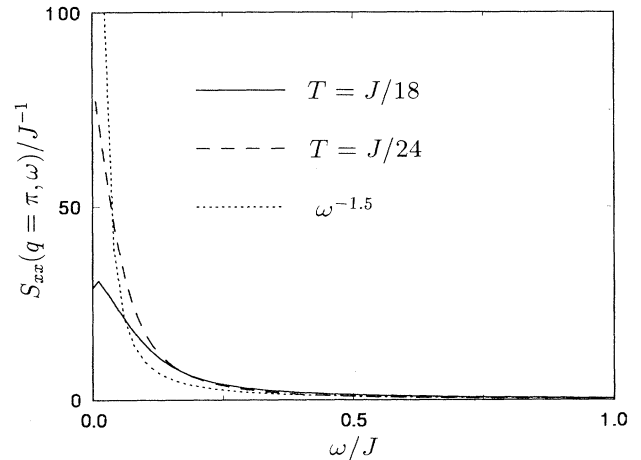


FIG. 7. Dynamic in-phase correlations,  $S_{xx}(q, \omega)$  for the  $xy$  model with  $q = \pi$ . As the temperature is lowered a sharper structure appears and approaches the  $\omega^{-1.5}$  dependence expected for  $T=0$ .

This continuum has a range given by

$$\frac{\pi J}{2} \sin|q| \leq \omega_q \leq \pi J \sin|q/2|. \quad (26)$$

Figure 8 shows the maximum entropy result. At  $q = \pi$  the full range of excitations from  $\omega = 0$  to  $\pi J$  appears in this spectrum with the spectral weight largest for low frequencies. This result agrees qualitatively with Müller, Beck, and Bonner's ansatz for  $S_{zz}(q, \omega)$ .<sup>10</sup>  $S_{zz}(q = \pi, \omega)$  peaks at a nonzero frequency because of finite-size effects.

When  $q$  decreases, the width of the spectrum decreases. This also agrees with Müller, Beck, and Bonner's ansatz.<sup>10</sup> A comparison of our results for  $S_{zz}(q = 3\pi/4, \omega)$  to this ansatz is made in Fig. 9. A substantial amount of the spectral intensity falls below the rigorous des Cloizeaux-Pearson cutoff at  $\omega = 1.1J$  because of maximum entropy broadening. This suggests that the spectral intensity is largest near the lower cutoff.

In summary, these results suggest that the following holds true for the one-dimensional  $S = \frac{1}{2}$  Heisenberg antiferromagnet: (1) spectral weight is found over the entire range described by Eq. (26) and (2) spectral weight is concentrated near the lower bound of that continuum. We note that in a previous paper<sup>12</sup> an explicit comparison was made between Monte Carlo results and inelastic neutron-scattering experiments for the  $S = \frac{1}{2}$  antiferromagnet  $\text{CuCl}_2\text{N}(\text{C}_5\text{D}_5)$  and good agreement was shown.

### B. $S = 1$

The existence of the Haldane gap for integer-spin one-dimensional Heisenberg antiferromagnets has been verified numerically by Nightingale and Blöte<sup>7</sup> and Takahashi<sup>8</sup> who find a gap of  $\Delta \sim 0.4J$  for  $S = 1$ . A recently developed lattice renormalization-group method yields a very precise figure of  $0.4105J$ .<sup>9</sup> Buyers *et al.*'s

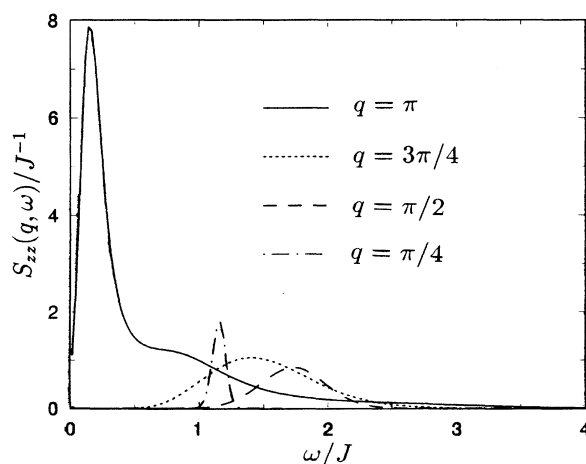


FIG. 8.  $S_{zz}(q, \omega)$  for the  $S = \frac{1}{2}$  Heisenberg model. The  $q = \pi$  spectrum is broad indicating the spin-wave continuum is accessible. The width of the continuum shrinks as  $q$  decreases.

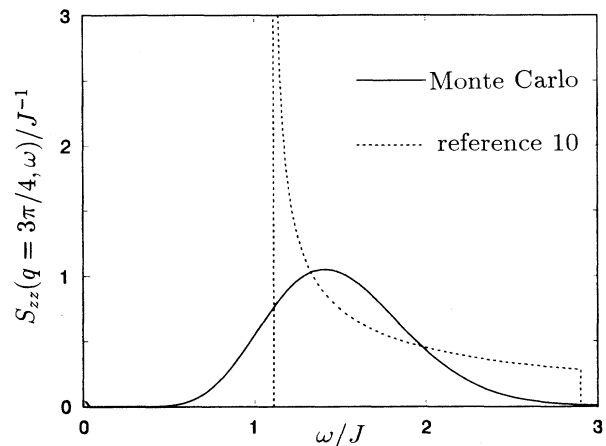


FIG. 9. Monte Carlo result for  $S_{zz}(q = 3\pi/4, \omega)$  versus the ansatz of Müller, Beck, and Bonner for the  $S = \frac{1}{2}$  Heisenberg model. Maximum entropy broadening places considerable weight below the rigorous lower cut-off at  $\omega = 1.1J$ . This suggests a large concentration of spectral weight near the lower boundary of the spin-wave continuum as found in the ansatz.

experimental results for  $\text{CsNiCl}_3$  agree with these results.<sup>3</sup>

The gap structure for  $S = 1$  is clearly displayed in Fig. 10. There is a striking difference between the  $q = \pi$  spectrum for  $S = 1$  and for  $S = \frac{1}{2}$ . The  $S = 1$  peak position of  $0.41J$  agrees with the expected value for the lowest-lying  $\Delta S_T = 1$  excitation. Note that  $S_{zz}(q = \pi, \omega)$  is symmetric about the point of maximum intensity. This strongly supports the idea that the spectrum is dominated by a single mode at  $\omega = 0.41J$  with the peak width due to max-

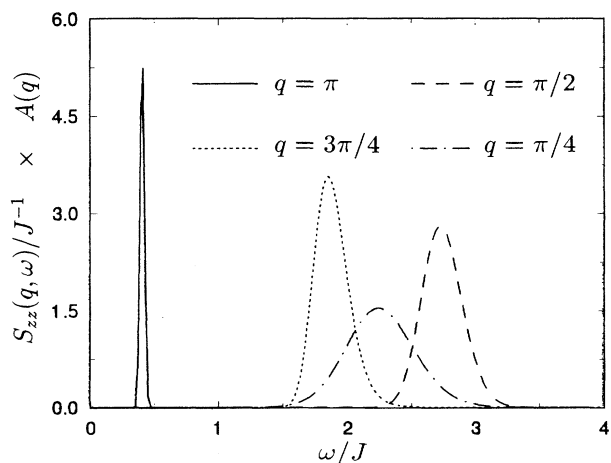


FIG. 10.  $S_{zz}(q, \omega)$  for the  $S = 1$  Heisenberg model. The gap in the spectrum is clearly observable and has a value of  $0.41J$ . In contrast to  $S = \frac{1}{2}$ ,  $S_{zz}(q, \omega)$  demonstrates single-mode behavior for  $q \geq \pi/2$ . For display purposes we have scaled the peaks by  $A(q) = 0.020, 0.45, 1.1, \text{ and } 3.1$  for  $q = \pi, 3\pi/4, \pi/2, \text{ and } \pi/4$ , respectively.

imum entropy broadening. Experimental data on NENP shows just such behavior for  $\pi/3 \leq q \leq \pi$ .<sup>27</sup> This contrasts with  $S = \frac{1}{2}$  where there is a continuum of excitations and  $S_{zz}(q = \pi, \omega)$  is asymmetric.

All results for  $q \geq \pi/2$  indicate that they are dominated by a single mode.  $S_{zz}(q = 3\pi/4, \omega)$  peaks near  $1.85J$ , which is close to the value Takahashi found ( $1.89J$ ), for the lowest-energy excitation with momentum  $q = 3\pi/4$ .<sup>8</sup> For  $q = \pi/2$  the peak frequency  $2.73J$  is also near Takahashi's result ( $2.66J$ ) for the lowest-energy excitation with  $q = \pi/2$ . Since spectral weight should not be found below the lowest excitation energy for  $T \rightarrow 0$ , the weight found below must be due to maximum entropy broadening. This broadening appears to place the same weight above the lowest-energy excitation as below. It seems likely, then, that the exact result is dominated by a single mode at the lowest energy of excitation for a given value of momentum.

For low  $q$  values the numerical results of Takahashi<sup>8</sup> suggest that the excitations are the result of two-magnon processes, that is, the lowest  $q = 0$  excitation energy is  $2\Delta$  resulting from the sum of two  $\omega = \Delta$ ,  $q = \pi$  magnons. Affleck and Weston have constructed a small  $q$  representation of  $S(q, \omega)$  assuming two-magnon excitations dominate the spectrum.<sup>28</sup> In contrast to what we find for large  $q$  values, Affleck and Weston predict that the spectrum spans a range of frequencies for small  $q$  with the maximum intensity at the lower edge of the continuum.

Our results for  $q = \pi/4$  suggests multimode behavior. The minimum excitation energy for  $q = \pi/4$  is  $2.04J$ ,<sup>8</sup> but our result peaks at  $2.24J$ . Further, following the procedure described in Sec. III A, we find that single mode data for  $\omega = 2.24J$  can be resolved to within  $0.35J$ , while the  $q = \pi/4$  peak width is  $0.7J$ . For  $q \geq \pi/2$  we find the single mode results to be consistent with  $S(q, \omega)$ .

The  $q = \pi/8$  result, shown in Fig. 11, is even more suggestive of multimode behavior. The peak position is

$1.44J$ , which is above the lowest mode energy  $1.32J$ . The long high-frequency tail is reminiscent of the spin-wave continuum observed for  $S = \frac{1}{2}$  at all momentum values. The  $q = \pi/8$  result is clearly distinguishable from the result that is obtained from single-mode data as is also shown in Fig. 11.

Another interesting phenomenon is the temperature dependence of the  $q = \pi$  peak position which is plotted in Fig. 12. The increase in  $\omega_{\text{peak}}$  with temperature has been observed in NENP (Ref. 29) and  $\text{CsNiCl}_3$ .<sup>30</sup> We were unable to resolve a peak for  $T \geq 0.5J$ . This may be due to maximum entropy broadening. However, the  $q = \pi$  peak for NENP becomes unobservable for  $T \geq 0.4J$ .<sup>29</sup> This suggests that a well defined peak is found only for  $T \leq \Delta$ .

### C. $S = \frac{3}{2}$

Figures 8 and 10 show that the spectra for  $S = \frac{1}{2}$  and 1 are distinct. As  $S$  increases the qualitative difference between integer and half-integer spin systems should become less pronounced. For  $S = \frac{3}{2}$  exact diagonalization studies are limited to small systems ( $\sim 12$  sites<sup>31</sup>), but our method is easily applied to 64-site systems.

$S_{zz}(q = \pi, \omega)$  for  $S = \frac{3}{2}$  is shown in Fig. 13. It is reminiscent of the  $S = \frac{1}{2}$  spectrum shown in Fig. 8. Namely, there is a continuum of excitations that extend to low-frequency cutoff, but is cutoff by the finite-size gap. The continuum is narrower for  $S = \frac{3}{2}$  than for  $S = \frac{1}{2}$ .  $S = \frac{3}{2}$  has spectral weight extending only to  $\omega \sim J$ , while  $S = \frac{1}{2}$  has substantial weight out to  $\omega \sim \pi J$ .

These results suggest the following  $S$  dependence for the spectra of spin excitations for one-dimensional half-integer spin Heisenberg antiferromagnets: The broad spectra found for  $S = \frac{1}{2}$  narrow as  $S$  increases. In the classical limit ( $S \rightarrow \infty$ ), where half-integer and integer-spin systems become alike, the spectrum consists of a single spin-wave mode at  $\omega_q = (2S + 1)J \sin q$ .

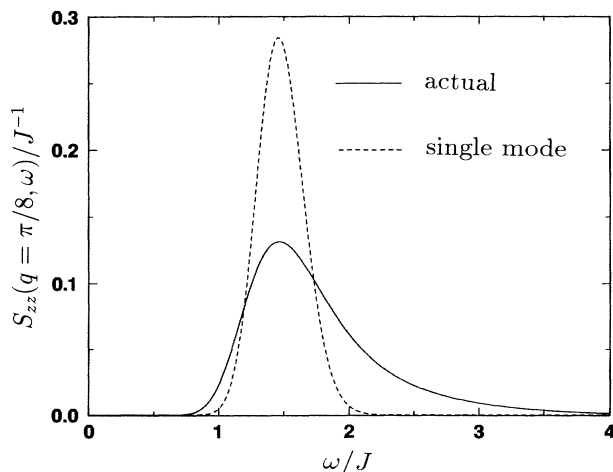


FIG. 11.  $S_{zz}(q = \pi/8, \omega)$ . The asymmetry of the line shape is evident, indicative of two-magnon excitations dominating this low  $q$  result. For comparison we include the result obtained when single-mode data is used for  $S(q, \tau)$ .

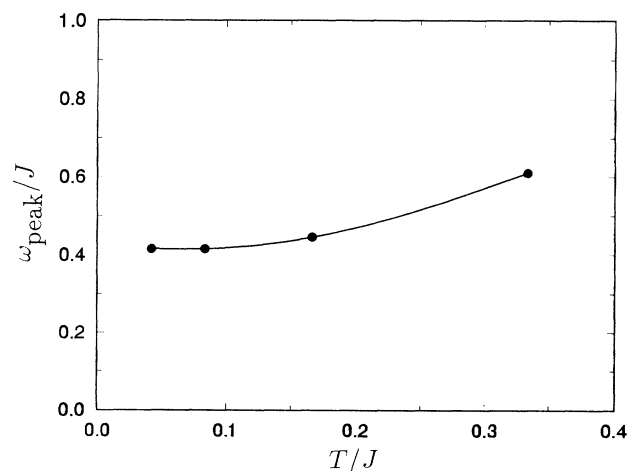


FIG. 12. Temperature dependence of the  $q = \pi$  peak position for  $S = 1$ . The upward dependence with temperature agrees with experimental result for  $\text{CsNiCl}_3$  and NENP.

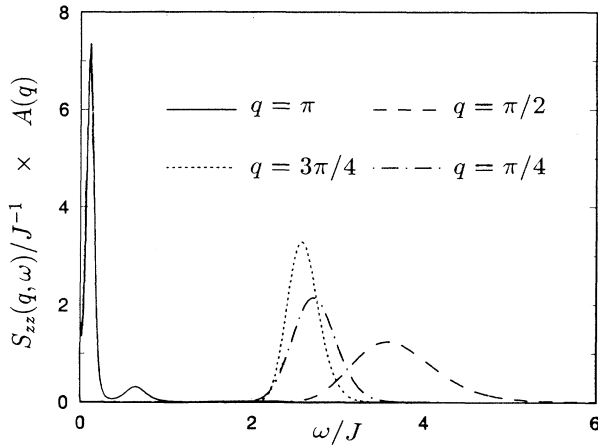


FIG. 13.  $S_{zz}(q, \omega)$  for the  $S = \frac{3}{2}$  Heisenberg model.  $q = \pi$  has a continuum of width  $\sim J$ . Results for lower  $q$  values are not accurate enough to distinguish from classical single-mode behavior.  $A(q) = 0.016, 0.42, 1.0,$  and  $2.5$  for  $q = \pi, 3\pi/4, \pi/2,$  and  $\pi/4$ , respectively.

Our results for  $S_{zz}(q, \omega)$  with  $q = 3\pi/4, \pi/2,$  and  $\pi/4$  appear to be symmetric about their peaks. Most likely, the exact results are asymmetric (like for  $q = \pi$ ), but as  $S = \frac{3}{2}$  peaks are more narrow than  $S = \frac{1}{2}$  peaks, the maximum entropy method is not accurate enough to detect the asymmetry. Indeed, we find that the apparent width of  $q < \pi$  is accounted for by maximum entropy broadening. The peak positions are all within 10% of  $(2S + 1)\text{sin}q$ . These  $S = \frac{3}{2}$  results suggest that within the accuracy of our method, the  $S(q, \omega)$  spectra for  $S \geq \frac{5}{2}$  will be indistinguishable from those obtained with classical simulations.<sup>32</sup>

#### D. $S = 2$

In the classical limit ( $S \rightarrow \infty$ )  $S_{zz}(q, \omega)$  is dominated by a single mode at  $\omega_q \sim (2S + 1)\text{sin}q$  for which  $\omega_q \rightarrow 0$  for  $q = \pi$  or 0.  $S = 1$  has a fairly large gap  $\Delta = 0.4J$ . It is of interest to produce an estimate of the  $S = 2$  gap. Haldane has shown that the size of the gap decreases like  $S^2 e^{-\pi S}$  in the limit  $S \rightarrow \infty$ ,<sup>6</sup> but it is not known how accurate this is for  $S = 1$  and 2.

In Fig. 14 the  $S = 2$  gap structure is clearly evident. For  $q = \pi$  a very sharp feature is observed at  $\omega = 0.115J$ . The large correlation length for  $S = 2$  ( $\xi \sim 80$ ) suggests that system sizes larger than the 64 sites used here are required to obtain the thermodynamic value for the gap. Figure 15 shows the gap  $\Delta_N$  versus  $1/N$  where  $N$  is the system size.  $T = J/36$  for all  $N$  and  $N$  is taken to be as large as 128 sites. Our best estimate for  $\Delta_\infty$ , the  $S = 2$  Haldane gap in the thermodynamic limit, is  $0.08J$  as suggested by the extrapolation of our data to  $1/N \rightarrow 0$ .

Our estimate for the ratio of the  $S = 2$  and 1 gaps is  $\sim 0.08J/0.41J = 0.20$ . Haldane's asymptotic formula yields

$$4 \exp(-2\pi) / \exp(-\pi) = 0.17$$

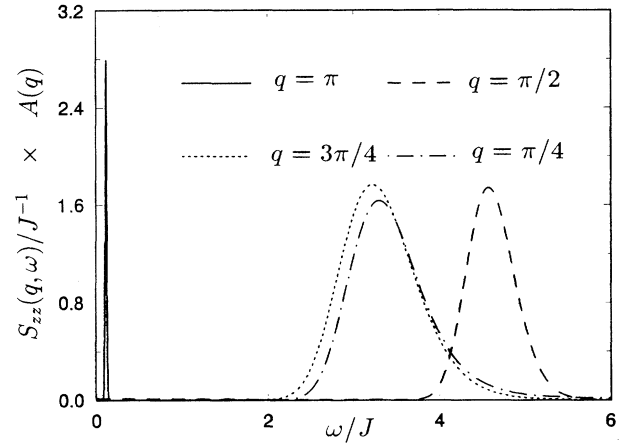


FIG. 14.  $S_{zz}(q, \omega)$  for the  $S = 2$  Heisenberg model. The  $q = \pi$  gap structure is evident along with single-mode behavior. Lower  $q$  values show results that are qualitatively similar to those for  $S = 3/2$ .  $A(q) = 5.0 \times 10^{-4}, 0.40, 0.66,$  and  $2.4$  for  $q = \pi, 3\pi/4, \pi/2,$  and  $\pi/4$ , respectively.

(Ref. 6). Although we have not performed the expensive calculations to prove so, we expect that the difference in the results is within the accuracy of our method. For example, it is possible that our result is affected by the finite size of  $\Delta\tau$  ( $\sim 0.25J^{-1}$ ) used in the Monte Carlo simulations. It is possible to go to higher temperature to use smaller  $\Delta\tau$  values, but the  $q = \pi$  peak position is strongly temperature dependent<sup>14</sup> like that for  $S = 1$  as is shown in Fig. 12.

It would be computationally expensive, although possible, to use this technique to obtain the gap for  $S = 3$  where  $\xi > 1000$ . However, Haldane's formula appears to be fairly accurate for  $S = 1$  and 2. This formula yields the fairly small value  $\Delta_{S=3} \approx 0.007J$  which would be a

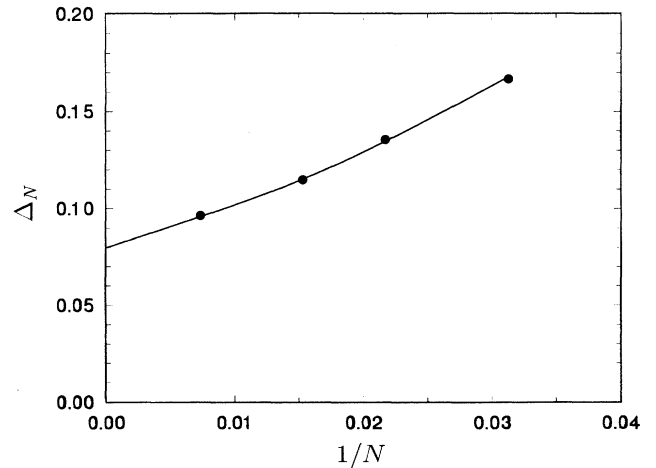


FIG. 15. Dependence of the gap  $\Delta_N$  on the number of sites,  $N$ , for  $S = 2$  and  $T = J/36$ . Extrapolating to  $1/N \rightarrow 0$  yields an estimate of  $0.08J$  for the gap in the thermodynamic limit.

challenge to obtain with this or any other method.

Results for momenta  $q=3\pi/4$ ,  $\pi/2$ , and  $\pi/4$  in Fig. 14 appear to be nearly identical with the corresponding  $S=\frac{3}{2}$  results except that the peaks are shifted approximately by a factor  $\sim\frac{5}{4}$  corresponding to the factor  $2S+1$  in the classical spin-wave theory prediction for the energy of the single mode. The qualitative differences between  $S=\frac{3}{2}$  and 2 for  $q\neq\pi$  are apparently too small to be detected with this method.

#### E. $S=1$ Heisenberg model with on-site anisotropy

$S_{xx}(q,\omega)=S_{yy}(q,\omega)=S_{zz}(q,\omega)$  for the isotropic Heisenberg model. Spin anisotropy is introduced by the spin-orbit interaction in a noncubic lattice. For weak spin-orbit coupling an effective Hamiltonian can be written in terms of spin degrees of freedom only as orbital degrees of freedom typically have higher-energy scales. One possibility is the Heisenberg Hamiltonian with on-site anisotropy

$$H=J\sum_i\mathbf{S}_i\cdot\mathbf{S}_{i+1}+D\sum_i(S_i^z)^2. \quad (27)$$

The on-site anisotropy term  $\sum_i D(S_i^z)^2$  will either favor having spins lying in the  $xy$  plane ( $D>0$ ) or along the  $z$  direction ( $D<0$ ). Previous theoretical study of Eq. (27) includes that of Botet, Jullien, and Kolb<sup>33</sup> who performed exact diagonalization studies on  $N\leq 12$  site systems. More recent work on larger systems (up to 32 sites) has been reported by Sakai and Takahashi<sup>34</sup> and Golinelli, Jolicoeur, and Lacaze.<sup>35</sup>

For  $S=\frac{1}{2}$  on-site anisotropy has no effect because  $(S_i^z)^2$  is always  $\frac{1}{4}$ . However, this term is relevant for  $S\geq 1$ . The  $S=1$  one-dimensional antiferromagnet NENP is believed to be described by Eq. (27) with  $J\approx 4.0$  meV and  $D=0.2J$ .<sup>27</sup>

Motivated by this assignment for NENP we take  $D/J=0.2$ . Figure 16 shows the resulting spectra for

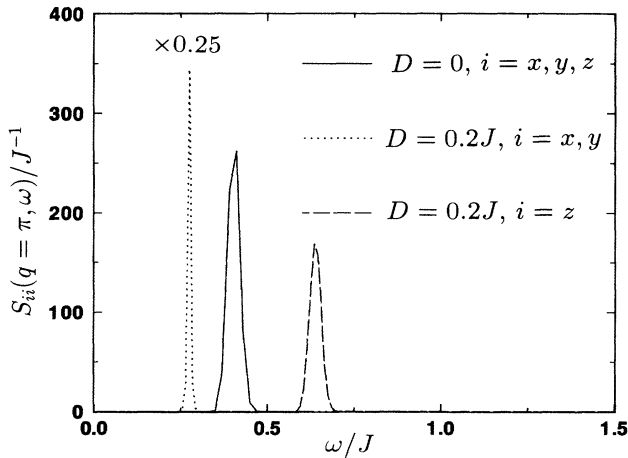


FIG. 16.  $S_{xx}(q=\pi,\omega)$  and  $S_{zz}(q=\pi,\omega)$  for the  $S=1$  Heisenberg model with on-site anisotropy. A gap splitting is observed which correlates well with the splitting for NENP. We obtain  $\Delta_x=0.28J$  and  $0.64J$ .

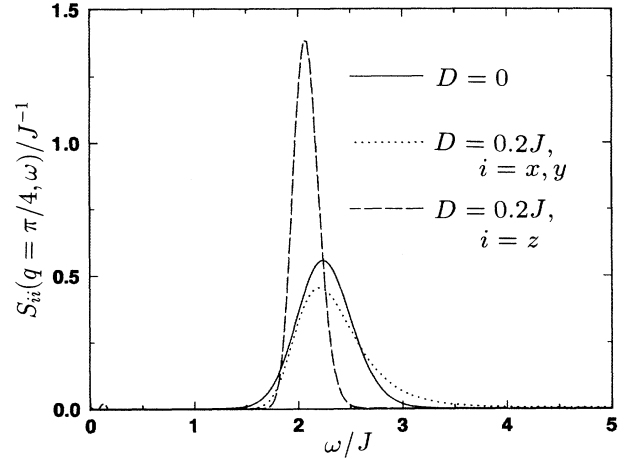


FIG. 17.  $S_{xx}(q=\pi/4,\omega)$  and  $S_{zz}(q=\pi/4,\omega)$  for the  $S=1$  Heisenberg model with on-site anisotropy. In contrast to  $q=\pi$ , the peak for  $S_{zz}(q=\pi/4,\omega)$  lies lower than the peak for  $S_{xx}(q=\pi/4,\omega)$ . The change in the relative positions of the peaks correlates with neutron-scattering results for NENP where the distinct peaks merge for  $q<0.8\pi$  with the small peak splittings being outside of the experimental resolution.

$q=\pi$ .  $S_{zz}(q,\omega)$  and  $S_{xx}(q,\omega)=S_{yy}(q,\omega)$  are shown along with the  $D=0$  result presented earlier. The Haldane gap structure is clearly preserved when anisotropy is included. The in-plane gap is reduced to  $\Delta_{xy}\approx 0.28J$  from the  $D=0$  value of  $0.4J$ . The out of plane gap is  $\Delta_z\approx 0.64J$ . For the same parameters Golinelli, Jolicoeur, and Lacaze obtain  $\Delta_{xy}\approx 0.29J$  and  $\Delta_z\approx 0.69J$  via extrapolation to the thermodynamic of results from finite-size lattices. The experimental results for NENP yield  $\Delta_{xy}=(0.275\pm 0.02)J$  and  $\Delta_z=(0.59\pm 0.04)J$  (Ref. 29) which are in the range of our values for  $D=0.2J$ .

In contrast to  $q=\pi$ , for  $q=\pi/4$ ,  $S_{zz}(q,\omega)$  has spectral weight at lower frequency than  $S_{xx}(q,\omega)$  (Fig. 17). The average moment

$$\langle\omega\rangle=\frac{\int_{-\infty}^{\infty}\omega S_{jj}(q,\omega)d\omega}{\int_{-\infty}^{\infty}S_{jj}(q,\omega)d\omega} \quad (28)$$

differs by 10% between  $j=x$  and  $z$  for  $q=\pi/4$ . This difference is well within the statistical accuracy of quantum Monte Carlo which, using the  $f$ -sum rule,<sup>36</sup> evaluates  $\langle\omega\rangle$  directly without recourse to the maximum entropy method. The neutron-scattering results of Ma *et al.*<sup>27</sup> shows two distinct peaks for  $q>0.8\pi$  and a single peak otherwise. This likely reflects the merging and crossing of the peaks as  $q$  decreases, which then appear as a single peak because of finite resolution.

#### V. SUMMARY AND FUTURE DIRECTIONS

This work combines the world-line quantum Monte Carlo and maximum entropy methods to obtain dynamical properties of strongly interacting one-dimensional spin systems. Results for the Ising and  $xy$  models results obtained with this dynamical method were compared to

exact results. This comparison shows that this dynamical method produces results that contain the correct qualitative features and represent a convolution of the exact results with a broadening function of broadening width  $\Delta\omega$  which is small at low frequencies, but is larger at high frequencies. Peak positions are accurately obtained.

The dynamical spin structure factor  $S_{zz}(q, \omega)$  for the antiferromagnetic Heisenberg model with  $S = \frac{1}{2}, 1, \frac{3}{2}$ , and 2 shows the difference between integer and half-integer spins as predicted by Haldane.<sup>6</sup> We obtain Haldane gaps of  $0.41J$  for  $S = 1$  and  $0.08J$  for  $S = 2$ ; the  $S = 1$  result agrees with previous results.<sup>7,8</sup> When on-site anisotropy is added to the  $S = 1$  Heisenberg antiferromagnet the calculated gap splitting is equivalent to the splittings for NENP.<sup>29</sup>  $S_{zz}(q, \omega)$  for  $S = \frac{1}{2}$  and  $\frac{3}{2}$  shows a broad continuum of excitations. This continuum shrinks when  $S$  increases from  $\frac{1}{2}$  to  $\frac{3}{2}$  and suggests the approach of the classical limit,  $S \rightarrow \infty$ , where  $S_{zz}(q, \omega)$  is dominated by a single frequency. We observe the  $q = \pi$  peak position for  $S = 1$  to increase with temperature as has been seen experimentally.

There are several possible avenues for future studies. Neutron-scattering studies are often performed in the presence of a static magnetic field. Unfortunately, this method can obtain  $S_{zz}(q, \omega)$  only when the applied field is in the  $z$  direction because of "minus sign" problems for the Monte Carlo. Affleck has suggested that the dynamical properties of  $S = 1$  chains may be particularly interesting in a field.<sup>37</sup> However, it appears that the most interesting features in  $S_{zz}(q, \omega)$  appear when the field is in the  $x$  or  $y$  directions.

This dynamical method can be applied to a more general class of nearest-neighbor Hamiltonians. Bonner has described the expected behavior for the Heisenberg mod-

el with anisotropic exchange<sup>38</sup>

$$H = \sum_i J_x S_i^x S_{i+1}^x + J_y S_i^y S_{i+1}^y + J_z S_i^z S_{i+1}^z . \quad (29)$$

For  $J_z > J_y = J_x \geq 0$  Ising order and subsequently an excitation gap develops for half-integer  $S$ , while gapless behavior persists for all  $J_x = J_y \geq J_z \geq 0$ . For integer  $S$  there is a range about  $J_x = J_y = J_z$  where an excitation gap is present. However, when  $J_z$  is below a critical value the gap is absent. All of these features can be studied with this dynamical method and estimates for the excitation gaps can be produced.

It would be interesting to study systems containing both half-integer and integer spins. Hagiwara *et al.* have studied the  $S = 1$  antiferromagnet NENP doped with a small amount of  $S = \frac{1}{2}$   $\text{Cu}^{++}$  impurities.<sup>39</sup> The spin dynamics of an  $S = \frac{1}{2}$  impurity in an  $S = 1$  chain is accessible with this method.

*Note added in proof.* Results similar to those found in Sec. IV E have been reported by Golinelli, Jolicoeur, and Lacaze [J. Phys. Condens. Matter 5, 1399 (1993)].

#### ACKNOWLEDGMENTS

We thank I. Affleck, N. Bonesteel, J. Gubernatis, C. Jayaprakash, D. Scalapino, R. Silver, S. White, and W. Wenzel for useful conversations. This work has been supported by NSF Grant Nos. DMR-8857341 and DMR-9107563 and a grant from the Cray Research Foundation. One of us (D.L.C.) thanks the A.P. Sloan Foundation for support. We gratefully acknowledge a grant of computer time from the Ohio Supercomputer Corporation.

\*Present address: Dept. of Physics, Georgetown University, Washington, D.C. 20057.

<sup>1</sup>Y. Endoh, G. Shirane, R. J. Birgeneau, Peter M. Richards, and S. L. Holt, Phys. Rev. Lett. **32**, 170 (1974).

<sup>2</sup>S. E. Nagler, D. A. Tennant, R. A. Cowley, T. G. Perring, and S. K. Satija, Phys. Rev. B **44**, 12 361 (1992).

<sup>3</sup>W. J. L. Buyers, R. M. Morra, R. L. Armstrong, M. J. Hogan, P. Gerlach, and K. Hirakawa, Phys. Rev. Lett. **56**, 371 (1986).

<sup>4</sup>J. P. Renard, M. Verdagner, L. P. Regnault, W. A. C. Erkelens, J. Rossat-Rignod, and W. G. Stirling, Eurphys. Lett. **3**, 945 (1987).

<sup>5</sup>H. Mutka, C. Payen, P. Molinié, J. L. Soubeyroux, P. Colombet, and A. D. Taylor, Phys. Rev. Lett. **67**, 497 (1991).

<sup>6</sup>F. D. M. Haldane, Phys. Lett. **93A**, 464 (1983); Phys. Rev. Lett. **50**, 1153 (1983); **61**, 1029 (1988).

<sup>7</sup>M. P. Nightingale and H. W. J. Blöte, Phys. Rev. B **33**, 659 (1986).

<sup>8</sup>M. Takahashi, Phys. Rev. Lett. **62**, 2313 (1989).

<sup>9</sup>S. R. White, Phys. Rev. Lett. **69**, 2863 (1992); S. R. White and D. A. Huse, Phys. Rev. B **48**, 3844 (1993).

<sup>10</sup>G. Müller, H. Beck, and J. C. Bonner, Phys. Rev. Lett. **43**, 75 (1979).

<sup>11</sup>H. J. Schultz and T. A. L. Ziman, Europhys. Lett. **18**, 355 (1992).

<sup>12</sup>J. Deisz, M. Jarrell, and D. L. Cox, Phys. Rev. B **42**, 4869 (1990).

<sup>13</sup>M. Makivić and M. Jarrell, Phys. Rev. Lett. **68**, 1770 (1992).

<sup>14</sup>J. Deisz, Ph.D. thesis, The Ohio State University, 1991.

<sup>15</sup>M. Suzuki, Commun. Math. Phys. **51**, 183 (1976); M. Barma and B. S. Shastry, Phys. Rev. B **18**, 3351 (1978); J. E. Hirsch, D. J. Scalapino, R. L. Sugar, and R. Blankenbecler, *ibid.* **26**, 5033 (1982).

<sup>16</sup>S. F. Gull and J. Skilling, IEEE Proc. F **131**, 646 (1984).

<sup>17</sup>R. N. Silver, D. S. Sivia, and J. E. Gubernatis, in *Quantum Simulations of Condensed Matter Systems*, edited by J. D. Doll and J. E. Gubernatis (World Scientific, Singapore, 1990), p. 340.

<sup>18</sup>J. E. Gubernatis, M. Jarrell, R. N. Silver, and D. S. Sivia, Phys. Rev. B **44**, 6011 (1991); M. Jarrell, J. Gubernatis, and R. N. Silver, *ibid.* **44**, 5347 (1991).

<sup>19</sup>M. Marcu, in *Quantum Monte Carlo Methods*, edited by M. Suzuki (Springer-Verlag, Berlin, 1987), p. 64.

<sup>20</sup>E. H. Lieb, T. Schultz, and D. J. Mattis, Ann. Phys. (N.Y.) **16**, 407 (1961).

<sup>21</sup>S. Katsura, T. Horiguchi, and M. Suzuki, Physica **46**, 67 (1970).

<sup>22</sup>B. McCoy, E. Barouch, and P. Abraham, Phys. Rev. A **4**, 2331 (1971).

- <sup>23</sup>A. Luther and I. Peschel, *Phys. Rev. B* **12**, 3908 (1975).
- <sup>24</sup>G. Müller, H. Thomas, M. W. Puga, and H. Beck, *J. Phys. C* **14**, 3399 (1981).
- <sup>25</sup>H. Bethe, *Z. Phys.* **71**, 205 (1931).
- <sup>26</sup>J. des Cloizeaux and J. J. Pearson, *Phys. Rev.* **128**, 2131 (1962).
- <sup>27</sup>S. Ma, C. Broholm, D. H. Reich, B. J. Sternlieb, and R. W. Erwin, *Phys. Rev. Lett.* **69**, 3571 (1992).
- <sup>28</sup>I. Affleck and R. A. Weston, *Phys. Rev. B* **45**, 4667 (1992).
- <sup>29</sup>J. P. Renard, M. Verdager, L. P. Regnault, W. A. C. Regnault, J. Rossat-Mignod, J. Ribas, W. G. Stirling, and C. Vetter, *J. Appl. Phys.* **63**, 3538 (1988).
- <sup>30</sup>Z. Tun, W. J. L. Buyers, R. L. Armstrong, K. Hirakawa, and B. Briat, *Phys. Rev. B* **42**, 4677 (1990); I. Affleck, *Phys. Rev. Lett.* **62**, 474 (1989).
- <sup>31</sup>D. Guo, T. Kennedy, and S. Mazumdar, *Phys. Rev. B* **41**, 9592 (1990).
- <sup>32</sup>M. Steiner, J. Villain, and C. G. Windsor, *Adv. Phys.* **25**, 87 (1976).
- <sup>33</sup>R. Botet, R. Jullien, and M. Kolb, *Phys. Rev. B* **28**, 3914 (1983).
- <sup>34</sup>T. Sakai and M. Takahashi, *Phys. Rev. B* **42**, 4537 (1990).
- <sup>35</sup>O. Golinelli, Th. Jolicœur, and R. Lacaze, *Phys. Rev. B* **45**, 9798 (1992).
- <sup>36</sup>Sum rules from P. C. Hohenberg and W. F. Brinkman, *Phys. Rev. B* **10**, 128 (1974) can be modified to take into account on-site anisotropy.
- <sup>37</sup>I. Affleck, *Phys. Rev. B* **41**, 6697 (1990); *J. Magn. Magn. Mater* **90&91**, 210 (1990).
- <sup>38</sup>J. C. Bonner, *J. Appl. Phys.* **61**, 3941 (1987).
- <sup>39</sup>M. Hagiwara, K. Katsumata, I. Affleck, B. I. Halperin, and J. P. Renard, *Phys. Rev. Lett* **65**, 3181 (1990).